

X-Rays From Massive OB Stars: Thermal Emission From Radiative Shocks

Svetozar A. Zhekov^{1*} and Francesco Palla^{2†}

¹ *Space Research Institute, Sofia-1000, Moskovska str. 6, Bulgaria*

² *INAF-Osservatorio Astrofisico di Arcetri, I-50125 Firenze, Italy*

ABSTRACT

Chandra gratings spectra of a sample of 15 massive OB stars were analyzed under the basic assumption that the X-ray emission is produced in an ensemble of shocks formed in the winds driven by these objects. Shocks develop either as a result of radiation-driven instabilities or due to confinement of the wind by relatively strong magnetic field, and since they are radiative, a simple model of their X-ray emission was developed that allows a direct comparison with observations. According to our model, the shock structures (clumps, complete or fractional shells) eventually become ‘cold’ clouds in the X-ray sky of the star. As a result, it is expected that for large covering factors of the hot clumps, there is a high probability for X-ray absorption by the ‘cold’ clouds, resulting in blue-shifted spectral lines. Our analysis has revealed that such a correlation indeed exists for the considered sample of OB stars. As to the temperature characteristics of the X-ray emission plasma, the studied OB stars fall in two groups: (i) one with plasma temperature limited to ~ 0.1 – 0.4 keV; (ii) the other with X-rays produced in plasmas at considerably higher temperatures. We argue that the two groups correspond to different mechanisms for the origin of X-rays: in radiation-driven instability shocks and in magnetically-confined wind shocks, respectively.

Key words: stars: early-type - stars: winds - X-rays: stars - shock waves

1 INTRODUCTION

The present concept on the origin of X-rays in massive OB stars posits that they are emitted by hot gas heated by shocks (Lucy & White 1980; Lucy 1982). OB stars possess massive and fast winds driven by radiation pressure (e.g. Castor, Abbott & Klein 1975) and subject to instabilities (radiation-driven instabilities, RDI, Owocki & Rybicki 1984) which may give rise to the formation of strong shocks (Owocki, Castor & Rybicki 1988; Feldmeier, Puls & Pauldrach 1997). The resulting emission is expected to be relatively soft (plasma temperatures $kT < 1$ keV), while the X-ray lines formed in the optically thick outflowing gas are predicted to be blue-shifted and asymmetric due to the different absorption of the red and blue part of the line profiles (Ignace 2001; Owocki & Cohen 2001).

Recently, it has been suggested that the presence of magnetic fields may be an important ingredient for the X-ray production mechanism in very young massive stars (Babel & Montmerle 1997; ud-Doula & Owocki 2002). The main physical effect of an ordered magnetic field is to chan-

nel the stellar wind towards the equatorial plane where the flows from the opposite stellar hemispheres collide, leading to the formation of strong shocks. The basic feature of the so-called magnetically-confined wind shock model (MCWS) is that the X-ray emission should be much harder (plasma temperatures $kT > 1$ keV) than that originating from the RDI shocks, and that the X-ray line profiles should be narrower (line widths as small as $\frac{1}{4}$ of the stellar wind velocity).

With the launch of the *Chandra* and *XMM-Newton* observatories, the quality of the X-ray data on OB stars has improved considerably, making it possible to test models of the origin of X-ray emission. Amongst the more than a dozen OB stars with gratings spectra of acceptable quality, only one object, ζ Puppis, shows unambiguous blueshifted spectral lines with asymmetric profiles (Cassinelli et al. 2001; Kahn et al. 2001). On the other hand, there are two objects, θ^1 Ori C (Schulz et al. 2000, 2003; Gagne et al. 2005) and τ Sco (Cohen et al. 2003), in which a clear manifestation of the MCWS effects is observed. While the scarcity of the MCWS-type objects might be accounted for by their youth and the expected decay of the magnetic field strength with the age of the massive star (Schulz et al. 2003), the standard RDI shock model needs further refinements to bring theory in accord with observations.

The fact that most OB stars show no appreciable line

* E-mail: szhekov@space.bas.bg

† E-mail: palla@arcetri.astro.it

shifts and asymmetric profiles is an obvious indication that their winds are much more transparent in X-rays than originally believed. This result, along with the small filling factors of the X-ray emitting plasma in OB stars as found in previous (*ROSAT*) studies (Kudritzki et al. 1996), lends support to a physical picture in which the stellar winds are clumpy and/or porous. Alternatively, if the winds are smooth and homogeneous, the mass-loss rates should have values appreciably smaller (a factor ~ 5 or more) than those presently accepted (Kramer, Cohen & Owocki 2003; Cohen et al. 2006).

Wind clumping and porosity effects on the X-ray emission from OB stars, and specifically on the shape of the line profiles, have been explored in recent analytical and numerical models (e.g., Feldmeier, Oskinova & Hamann 2003; Oskinova, Feldmeier & Hamann 2004, 2006; Owocki & Cohen 2006). It has been shown that under given conditions (such as reduced mass loss and assumed ‘typical’ distance between clumps) their inclusion may lead to results much more consistent with the observations. Given the complexity of these models and the fact that they are not yet fully self-consistent, it is important to gather empirical information about the physical conditions in the regions responsible for the X-ray emission to put further constraints on numerical models.

Various diagnostics have been used in this respect: analysis of helium-like triplet ratios, global fits with discrete-temperature models, constructing a distribution of emission measures as function of temperature, based on fits to individual-line fluxes and to the total X-ray spectra (Cassinelli et al. 2001; Kahn et al. 2001; Waldron & Cassinelli 2000; Miller et al. 2002; Cohen et al. 2003; Schulz et al. 2003; Sanz-Forcada, Franciosini & Pallavicini 2004; Wojdowski & Schulz 2004, 2005; Gagne et al. 2005; Leutenegger et al. 2006). These studies indicate that X-rays are produced close to the stellar surface (likely, in the wind acceleration zone), and that the corresponding hot plasma has a temperature stratification. The latter point reinforces the idea that the X-ray emission originates in an ensemble of shocks.

Guided by this background, we have developed a simple model which bears all the basic characteristics of the X-ray production in wind shocks. The model is described in § 2; the data sample is given in § 3; the results are presented in § 4 and discussed in § 5. The conclusions close the paper.

2 MODEL

As in the case of the RDI and MCWS models, our basic assumption is that the X-ray emission of hot massive stars originates in shocks. Given the relatively high densities in the wind, the energy losses by the shock-heated plasma are considerable: thus, shocks should be *radiative*. This conclusion follows from simple estimates which show that the typical cooling time of a parcel of gas at the postshock temperature and density is smaller than the typical dynamic time of the flow. Namely, for the shock position at a distance r from the star, the ratio of the cooling time ($t_c = \frac{5}{2} p_{sh}/Q_c$) to the dynamic time of the flow ($t_d = r/v$) is:

$$\frac{t_c}{t_d} = 1.58 \times 10^{-2} T_{sh}^{1.6} \left(\frac{r}{R_\odot} \right) v_{1000}^2 \dot{M}_6^{-1} \quad (1)$$

and the ratio of the thickness of the radiative shock (i.e., the cooling length of a parcel of hot gas at the postshock temperature: $l_c = \frac{1}{4} v_{sh} t_c$) and shock ‘radius’ is:

$$\frac{l_c}{r} = 3.59 \times 10^{-3} T_{sh}^{2.1} \left(\frac{r}{R_\odot} \right) v_{1000} \dot{M}_6^{-1} \quad (2)$$

where T_{sh} is the postshock temperature given in keV, v_{1000} is the terminal stellar wind velocity (in units of 1000 km s⁻¹), and \dot{M}_6 is the stellar mass loss (in units of 10⁻⁶ M_⊙ yr⁻¹). For a strong shock, the relation between the postshock temperature (in keV) and the shock velocity (in units of 1000 km s⁻¹) is given by $T_{sh} = 1.956 \mu v_{sh}^2$, and μ is the mean atomic weight. The relative number density of hydrogen is assumed $x_H = 0.9$; thus, the relative electron number density is $x_e = 1.1$ for a fully ionized plasma. The gasdynamical quantities and the cooling function are described in § 2.1.

For typical mass-loss rates ($\dot{M}_6 \approx 0.1 - 1$) and wind velocities ($v_{1000} \approx 1.5 - 2.5$), the cooling time and cooling length of a shock developed in a wind are appreciably smaller than the corresponding typical characteristics of the flow (see eqs. [1], [2]). This is true for postshock temperatures below 1 keV (i.e., shock velocities smaller than 1000 km s⁻¹ for solar abundances) and shock locations from a few to several tens of stellar radii. Therefore, the assumption of a steady-state, plane-parallel, radiative shock is a good approximation for our analysis. This conclusion finds support in numerical simulations of both the RDI and MCWS models. In fact, as a result of efficient cooling, the shocks ‘collapse’ in geometrically thin shells and disk-like structures, respectively (e.g. Feldmeier, Puls & Pauldrach 1997; ud-Doula & Owocki 2002; Gagne et al. 2005).

The description of our shock model and the ensemble of shocks is given below. The models were then used in the recent version (11.3.2) of the software package for analysis of X-ray spectra, XSPEC (Arnaud 1996). A global-fit approach was adopted in our analysis for the following reasons: (i) the fit can automatically take into account the quasi-continuum due to numerous weak lines; (ii) by fitting the shape of the underlying continuum, the model places additional constraints on the plasma temperature; (iii) the model can constrain the column density of the X-ray absorbing gas; and (iv) it can yield estimates of relative element abundances. Finally, the X-ray emission is assumed to originate from a hot optically-thin plasma in collisional ionization equilibrium (CIE), as is the case for various types of astrophysical objects, including hot massive stars (e.g., Paerels & Kahn 2006).

2.1 Shock Model

We consider a steady-state, plane-parallel, *radiative* shock moving in a gas with adiabatic index $\gamma = 5/3$. The basic physical quantities of the flow (density or nucleon number density, velocity, and pressure) have their standard postshock values for a strong shock: $\rho_{sh} = 4\rho_0$ ($n_{sh} = 4n_0$), $v_{sh} = v_0/4$, and $p_{sh} = 3/4\rho_0 v_0^2$, where the subscript ‘0’ denotes the preshock values (the gas velocity is given in the rest frame of the shock front). The mass and momentum conservation equations that describe the downstream flow are: $\rho v = \rho_{sh} v_{sh} = \rho_0 v_0$ ($n v = n_{sh} v_{sh} = n_0 v_0$), $\rho v^2 + p = \rho_0 v_0^2$,

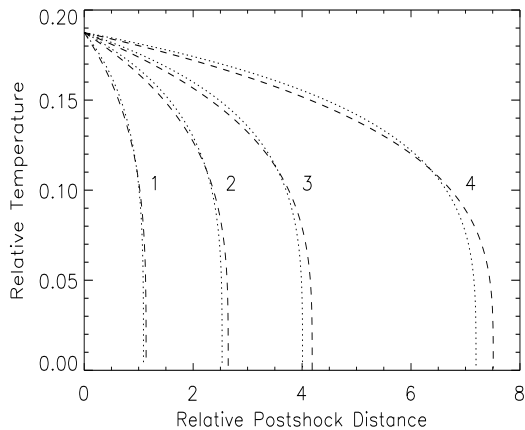


Figure 1. Temperature profile in a steady-state radiative shock. Dotted lines denote the exact solution, while the dashed ones give the approximate solution under constant-pressure assumption. The four curves are for shock velocities of 500, 650, 750 and 900 km s^{-1} , as correspondingly labeled: 1, 2, 3, and 4.

while the energy equation reads:

$$\frac{d}{d\xi} \left(\frac{\gamma}{\gamma-1} pv + \frac{\rho v^3}{2} \right) = -Q_c$$

where ξ is the distance downstream from the shock front, and Q_c is the cooling due to the optically thin, hot plasma in CIE.

In the steady-state case when cooling is efficient, the temperature decreases and the density increases downstream from the shock front. The cooling layer eventually ‘collapses’; that is, the gas velocity asymptotically reaches zero. It follows (see the momentum equation) that the gas pressure does not experience large variations in the postshock plasma ($3/4 \leq p/\rho_0 v_0^2 \leq 1$). Thus, we adopt a constant-pressure approximation (CPA) to describe the physical parameters of the postshock plasma. As we will see below, this allows us to easily make use of the radiative shock model in the analysis of the X-ray emission. Under the CPA, the energy equation reads:

$$\frac{5}{2}(1+x_e)nvk \frac{dT}{d\xi} = -x_e x_H n^2 \Lambda(T) \quad (3)$$

where the cooling term is given explicitly, T is the plasma temperature, k is the Boltzmann constant, $x_e = n_e/n$ is the relative electron number density, $x_H = n_H/n$ is the relative number density of hydrogen, and $\Lambda(T)$ is the cooling function at CIE (e.g. Raymond, Cox & Smith 1976). To facilitate the calculations, we followed a standard approach and made use of a piece-wise power-law approximation to the cooling curve: $\Lambda(T) = \Lambda_0 T^\alpha$. In the high-temperature intervals ($10^5 \leq T \leq 4 \times 10^7$, and $T \geq 4 \times 10^7$) the adopted values of the constants are $\Lambda_0 = 7 \times 10^{-19}$, 3×10^{-27} and $\alpha = -0.6, 0.5$ (e.g., Myasnikov, Zhekov & Belov 1998).

Figure 1 shows a comparison between the exact and the CPA solutions for the radiative shock and illustrates that our choice (CPA) is acceptable for the purpose of the present study. Moreover, as we will see below, the CPA allows an easy incorporation of the radiative shock model in

XSPEC which, unfortunately, is not the case for the exact solution of the problem.

To determine the X-ray spectrum from a steady-state, plane-parallel, radiative shock (with ‘surface’ A), we must integrate the hot plasma emissivity over a range of plasma temperatures in the temperature-stratified postshock zone (Fig. 1):

$$Sp(E) = A \int_0^{T_{sh}} \epsilon(E, T) x_e x_H n^2 d\xi \quad (4)$$

where $\epsilon(E, T)$ is the specific emissivity at given photon energy E and plasma temperature T (its integral over the entire energy/spectral range gives the value of the cooling curve at T), ξ is the distance from the shock front, and T_{sh} is the postshock temperature in keV. Then, using eq. (3), we can write:

$$Sp(E) = \Gamma_{sh} \int_0^{T_{sh}} \epsilon(E, T) T^{1-\alpha} d \ln T \quad (5)$$

where for numerical convenience we integrate over $\ln T$ instead of T , and Γ_{sh} is the normalization parameter. In this form, the X-ray spectrum from a radiative shock is well suited for modelling with XSPEC: namely, we simply have a known power-law distribution of emission measure at various temperatures, and we adopt an optically-thin plasma model (model *vapec* in XSPEC) for the plasma spectrum at temperature T (given by the quantity $\epsilon[E, T]$). Thus, our XSPEC shock model have the following parameters: the postshock temperature T_{sh} , chemical abundances and the normalization factor Γ_{sh} , which is related to the total emission measure in the shock (some technical details are found in Appendix A).

2.2 Global Model

Our global model assumes that X-rays are produced in radiative shocks which are randomly (and uniformly) distributed in the stellar wind, most likely in the acceleration zone. Therefore, the spectral lines in the total (integrated) X-ray spectrum from shocks are broadened by the bulk (wind) gas velocity, but are not shifted without including absorption. Qualitative physical considerations, also demonstrated by numerical modelling (e.g., Owocki & Cohen 2001), show that the X-ray absorption effects in the stellar wind result in blueshifted spectral lines with asymmetric line profiles.

To describe this physical situation we have constructed a new XSPEC model, whose technical aspects are given in Appendix A. The main features of the model are: (1) shocks are characterized by their postshock temperature and the distribution of the total emission measures in the shocks is determined from the Chebyshev polynomial algorithm, as is used in the standard XSPEC model *cbpvmkl* (Lemen et al. 1989). We note that a similar approach was successfully adopted in fitting the X-ray emission from an ensemble of adiabatic shocks (Zhekov et al. 2006). (2) The basis vectors for X-ray emission from the shock ensemble are those from the radiative shock model incorporated in XSPEC (see § 2.1). (3) All shocks have the same elemental abundances and share the same spectral line shifts. Thus, the basic model parameters are: the distribution of emission

Table 1. OB stars with *Chandra* Grating Spectra

No.	HD	Name	Type ^a	Distance ^b (pc)	Observation IDs	Counts ^c (MEG)	Data ^d
1	150136		O3	1300	2569	8569	8
2	66811	ζ Pup	O4 I	450	640	17435	1, 11
3	37022	θ ¹ Ori C	O4-6p	450	3, 4	28719; 13706	3, 6, 7, 11
4	149757	ζ Oph	O9V	140	2571, 4367	5915	
5	36486	δ Ori A	O9.5 II	501	639	6116	4, 11
6	37742	ζ Ori A	O9.7 Ib	501	610	9220	10, 11
7	37128	ε Ori	B0Iab:	412	3753	6811	
8	149438	τ Sco	B0.2 V	132	638	16838	2, 11
9	206267A		O6.5 V	800	1888, 1889	1597	5, 11
10	47839	15 Mon	O7 V	767	5401, 6247	1631	
11	57061	τ CMa	O9 II	1480	2525, 2526	1470	5, 11
12	37043	ι Ori	O9 III	440	599, 2420	4934	11
13	37468	σ Ori AB	O9.5 V	353	3738	1893	9
14	111123	β Cru	B0.5 III	110	2575	1830	11
15	116658	Spica	B1 III-IV	80	4509	3041	

^a Spectral type is from Wojdowski & Schulz (2005) except for HD 150136, ζ Oph, ε Ori, 15 Mon, σ Ori AB, and Spica whose spectral type is from SIMBAD.

^b Values of the distance are taken from Wojdowski & Schulz (2005) except for HD 150136 (Herbst & Havlen 1977), and ζ Oph, ε Ori, 15 Mon, σ Ori, and Spica (from the Jim Kaler’s ‘STARS’ web site: <http://www.astro.uiuc.edu/~kaler/sow/sowlist.html>).

^c The total number of counts in the *Chandra* MEG background-subtracted spectra. Thanks to the X-ray brightness of θ¹ Ori C, the two observations were analyzed separately. The data for Spica were obtained with the *Chandra* LETG.

^d References to the articles where the X-ray spectra of the stars are discussed in detail: (1) Cassinelli et al. (2001); (2) Cohen et al. (2003); (3) Gagne et al. (2005); (4) Miller et al. (2002); (5) Schulz (2003); (6) Schulz et al. (2000); (7) Schulz et al. (2003); (8) Skinner et al. (2005); (9) Skinner et al. (2007, in preparation); (10) Waldron & Cassinelli (2000); (11) Wojdowski & Schulz (2005).

measure of radiative shocks; chemical abundances, and the global line shift for the spectrum.

The profile asymmetry is handled through two (half)Gaussians each approximating the blue- and red-halves of the line profile. The Gaussian widths can vary with wavelength (in the same manner as in the XSPEC model *gsmooth*: $\Delta E \propto E^\beta$). Although the goal of our approach is just to obtain best fits to the line profiles over the entire spectrum, it is worth noting that the wavelength dependence of the line width represents the physical notion that faster shocks produce higher-temperature plasma whose emission is dominated by lines at shorter wavelengths.

3 X-RAY DATA

For our study, we selected a sample of OB stars with available gratings observations in the *Chandra* data archive. We extracted first-order spectra for each object according to the procedure described in the Science Threads for Grating Spectroscopy in the CIAO 3.3¹ data analysis software. The ancillary response functions for all spectra were generated using the *Chandra* calibration database CALDB v3.2. Table 1 gives some basic information about the stars of the sample and the X-ray observations. Our analysis is based on

the MEG spectra to take advantage of their higher sensitivity compared to the HEG spectra. One object (Spica) was observed with the *Chandra* LETG.

Depending on the quality of the data (the total number of photons), the MEG spectra were rebinned to have between 15 and 30 counts per bin. The spectra near the intercombination and the forbidden lines in the helium-like triplets (Si XIII, Mg XI, Ne IX and O VII) were rebinned so that these two lines fall into one large bin. This technical approach is aimed at improving the quality of the fit when optically thin plasma models (as those available in XSPEC) are used that do not take into account the effects of a strong external UV field. In the case of hot massive stars, such a UV field is present and it may alter the ratio of the two lines in the helium-like triplets, although it does not change their sum (the total emissivity/intensity). Thus, this technical approach allows to preserve the piece of information available in the helium-like triplets that can contribute in constraining some plasma characteristics (e.g., plasma temperature, abundances) which come out from the spectral fits.

4 RESULTS

The X-ray spectra (MEG) of the stars from our sample (see Table 1) were fitted with the global model that assumes a distribution of radiative shocks in the stellar wind (§ 2.2). To determine the elemental abundances, we varied only those having strong emission lines in the observed spectrum of a

¹ Chandra Interactive Analysis of Observations (CIAO), <http://cxc.harvard.edu/ciao/>

given object. These usually include N, O, Ne, Mg, Si and Fe, while for some objects C and S were also varied. For the abundance of all the other elements, the solar value was adopted (Anders & Grevesse 1989). Finally, to derive the X-ray absorption column density toward each object, we made use of Morrison & McCammon (1983) cross sections (XSPEC model *wabs*).

Table 2 presents some basic results from the fits to the spectra of the studied stars: the total χ^2 and the degrees of freedom for the fit (2nd column); the X-ray absorption column density (3rd column); the individual elemental abundance relative to the solar value (columns 4-10); the observed and unabsorbed X-ray flux (last columns). And the corresponding distributions of emission measure of the radiative shocks in the stellar winds are shown in Figure 2. The quality of the global fits in the vicinity of some strong emission lines is illustrated in Figure 3. A few properties are worth noting.

There is an indication that the metal abundances are subsolar in the sample of OB stars with gratings spectra and this trend is well demonstrated by the iron abundance being a factor of 2-3 below the solar value. Nitrogen might be considered an exception but we note that the poor quality of the data in the soft part of the X-ray spectra, where the nitrogen lines are found, prevents a firm conclusion. The values of the column density of the X-ray absorption material are consistent with those derived from the visual extinction to each object, using data from Berghöfer, Schmitt & Cassinelli (1996) and the Gorenstein (1975) conversion formula. The only object showing a clear sign of excess absorption with respect to its interstellar value is ζ Pup which may suggest that wind absorption effects play an important role in this object.

We see that most stars display the same distribution of emission measure of the radiative shocks, peaked at ~ 0.1 - 0.4 keV and with a very low level of high temperature tail extending above 1.0 keV. Thus, in most cases X-rays are produced in low velocity shocks. This finding is consistent with the radiation-driven instabilities scenario. The two most notable exceptions are θ^1 Ori C and τ Sco. In the former case, the main peak is at energy ~ 4 - 5 keV with a weaker component at ~ 0.8 keV. The case of τ Sco is more peculiar since there appear to be three peaks: one at very low energies, the main one at ~ 0.7 keV, and some emission above ~ 3 keV. One could argue that the hot tail in the distribution of emission measure in these objects is due to the MCWS while the cool component comes from the RDI shocks. For example, the shape of the emission measure distribution in θ^1 Ori C is stable between the two data sets (taken at two different times) and only the total amount of the hot gas changed mostly in the high-temperature component (Fig. 2). We note that this finding is in accord with the previous analysis of *Chandra* data (Schulz et al. 2003; Gagne et al. 2005). Such a different behaviour of the hot and cool components might be an indication of their different origin, as mentioned above. However, it is necessary to obtain more data also on τ Sco, in order to establish whether such a behaviour is typical only for one object or has much more general validity. It should be noted that there is a third object in our sample of OB stars, ζ Oph, whose distribution of radiative shocks is relatively ‘hot’ and it peaks at $\sim 0.5 - 0.6$ keV.

The presence of considerably hotter plasma (therefore,

fast velocity shocks), as definitely seen in θ^1 Ori C, τ Sco and ζ Oph, in combination with the relatively narrow lines observed in their spectra could be assumed as a clear manifestation of the magnetically-confined wind effects. It was recently proposed by Schulz et al. (2003) that the efficiency of the MCWS mechanism correlates with the age of the massive star. The relative youth of the first two objects (0.3 and ~ 1 Myr, see their Table 4) and the small kinematic age of ζ Oph (~ 1 Myr, Hoogerwerf, de Bruijne & de Zeeuw 2001) indeed support this suggestion.

5 DISCUSSION

The radiative shock model introduced in this study allows us to deduce some important information on the global physical state of the X-ray emitting region of massive stars. As one can see from eq. (A1), the normalization factor of the flux, Γ_{sh} , depends on the shock temperature (T_{sh}), stellar wind parameters (\dot{M}_6 , v_{1000}), and distance to the object in kpc (d_{kpc}): $\Gamma_{sh} = 2.444 \delta \left(\frac{\dot{M}_6}{v_{1000}} \right) \frac{\sqrt{T_{sh}}}{d_{kpc}^2}$, as δ gives the effective surface of the shock. Thus, from the results of the fits to the X-ray spectra, namely, using the Γ_{sh} value and knowing the distance to each star, we can deduce some useful information on the structure of the stellar winds. To do so, we introduce a new quantity, $\delta \left(\frac{\dot{M}_6}{v_{1000}} \right)$, that is related to a specific shock, or to a group of shocks with the same velocity. We will refer to this quantity as the specific stellar ‘cloudiness’.

In our picture, the winds of hot massive stars are clumpy and the clumps are likely generated by radiation-driven instabilities, particularly efficient in the inner acceleration zone. The instabilities develop into strong shocks which are the source of X-rays. Since the shocks are radiative, the gas density in the cooling zone is much larger (probably by a factor of a few tens and more) than the local density of the smooth wind. Away from the acceleration zone, these shock structures (clumps, complete or fractional shells) expand and cool down even further, but the density contrast in their ‘tail’ zone will remain appreciably high. Eventually, the clumps become ‘cold’ clouds in the X-ray sky of the hot massive star, and in a steady-state picture there will be a correlation between their characteristics: e.g., the higher the number of the hot clumps, the more numerous the ‘cold’ clouds; the higher the clumps’ covering factor, the higher the chance for X-ray absorption by the ‘cold’ clouds. In such a picture, the X-rays emitted from a particular shock will likely experience some absorption by the cold gas in its cooling zone, and there is a chance for more X-ray absorption to take place in the ‘cold’ tails of the other shocks and the ‘cold’ clouds as well. Although the exact situation depends on many specific details as the gas density in the clouds and their covering factor, it is anyway suggestive that the X-rays emitted from the ‘far side’ of the stellar wind (as seen by an observer) have a higher chance to suffer absorption than those emitted from the ‘near side’. Therefore, the emergent X-ray emission might be altered appreciably, resulting in a blue-shift of the spectral lines.

The specific stellar ‘cloudiness’ defined above is proportional to the quantities that determine the X-ray absorption efficiency of the cooling zones in the clumps and the cold clouds: namely, the geometrical extension of a cloud (the

Table 2. Shock Fitting Results (MEG 1-st order spectra)

Name	χ^2/dof	$N_H^{(a)}$	N	O	Ne	Mg	Si	S	Fe	$F_X^{(b)}$
HD 150136	146/335	4.2 ± 0.6	1	0.38 ± 0.13	0.47 ± 0.09	0.66 ± 0.10	0.85 ± 0.11	0.97 ± 0.31	0.35 ± 0.09	3.9 (24.4)
ζ Pup	491/433	3.7 ± 0.2	1.69 ± 0.33	0.16 ± 0.23	0.38 ± 0.03	0.54 ± 0.04	0.85 ± 0.06	1.36 ± 0.32	0.34 ± 0.03	12.0 (152.)
θ^1 Ori C ^c	776/1078	4.5 ± 0.3	1	0.79 ± 0.22	0.68 ± 0.07	0.83 ± 0.06	1.05 ± 0.08	1.11 ± 0.11	0.59 ± 0.04	26.0 (53.0)
ζ Oph	111/223	0.0 ± 0.9	1.43 ± 0.63	0.21 ± 0.05	0.51 ± 0.09	0.56 ± 0.1	0.65 ± 0.11	1	0.32 ± 0.05	5.7 (5.7)
δ Ori A	179/241	0.0 ± 0.9	0.35 ± 0.17	0.27 ± 0.07	0.45 ± 0.09	0.51 ± 0.11	0.53 ± 0.12	0.99 ± 2.26	0.31 ± 0.06	10.7 (10.7)
ζ Ori A	209/234	0.1 ± 0.3	0.23 ± 0.09	0.23 ± 0.04	0.44 ± 0.07	0.58 ± 0.09	0.63 ± 0.11	1.48 ± 1.64	0.36 ± 0.06	16.4 (18.5)
ϵ Ori	130/256	0.1 ± 0.4	0.33 ± 0.12	0.21 ± 0.04	0.39 ± 0.06	0.47 ± 0.08	0.58 ± 0.12	1	0.30 ± 0.05	11.5 (13.0)
τ Sco	503/420	0.0 ± 0.4	1.18 ± 0.30	0.29 ± 0.04	0.59 ± 0.06	0.63 ± 0.06	0.65 ± 0.06	0.78 ± 0.24	0.44 ± 0.04	16.8 (16.8)
HD 206267A	16/85	2.9 ± 1.6	1	0.20 ± 0.16	0.27 ± 0.16	0.49 ± 0.26	0.61 ± 0.32	1	0.22 ± 0.16	1.1 (8.4)
15 Mon	25/83	0.2 ± 1.4	1	0.31 ± 0.15	0.59 ± 0.33	0.64 ± 0.56	0.76 ± 1.21	1	0.56 ± 0.36	2.5 (3.0)
τ CMa	21/122	0.0 ± 1.8	1.16 ± 1.99	0.60 ± 0.60	0.71 ± 0.60	0.68 ± 0.60	1	1	0.49 ± 0.44	1.4 (1.4)
ι Ori	134/201	0.0 ± 1.0	0.79 ± 0.36	0.39 ± 0.11	0.64 ± 0.15	0.71 ± 0.18	1	1	0.56 ± 0.14	10.8 (10.8)
σ Ori	47/141	0.0 ± 1.8	1	0.44 ± 0.26	0.87 ± 0.50	0.94 ± 0.57	1	1	0.83 ± 0.49	2.3 (2.3)
β Cru	46/132	0.0 ± 1.9	0.29 ± 0.23	0.14 ± 0.08	0.30 ± 0.16	0.21 ± 0.17	1	1	0.33 ± 0.19	5.0 (5.0)
Spica ^d	97/152	0.0 ± 0.1	0.04 ± 0.07	0.09 ± 0.03	0.23 ± 0.08	0.20 ± 0.22	0.16 ± 0.06	0.42 ± 0.36	0.22 ± 0.09	1.5 (1.5)

Fit results from the XSPEC model: *wabs(gsm)* (*gsm* states for the global shock model as described in § 2.2). Derived for the each object emission measure distributions of radiative shocks are given in Fig. 2. The errors in the Table are 1σ . All abundances are expressed as ratios to their solar values (Anders & Grevesse 1989). Those without associated errors were kept fixed at their solar value.

^a The X-ray column density is in units of 10^{21} cm^{-2} .

^b Flux units are $10^{-12} \text{ ergs cm}^{-2} \text{ s}^{-1}$. The observed X-ray flux (0.3 - 8 keV) is followed in parentheses by the unabsorbed value.

^c The results are from a simultaneous fit to the both observations of this object. Such a model shares the same abundances for the both spectra and the other model parameters were varied individually for each data set. The values for the column density and the X-ray flux in the Table are for ObsId 3 while those for ObsId 4 are $N_H = 4.6 \pm 0.4$ and $F_X = 19.0$ (40.4). Abundances not given in the Table but also varied are: Ar = 1.42 ± 0.29 and Ca = 1.84 ± 0.47 .

^d The model fit is to the 1-st order LETG spectrum. Carbon abundance is C = 0.22 ± 0.10 .

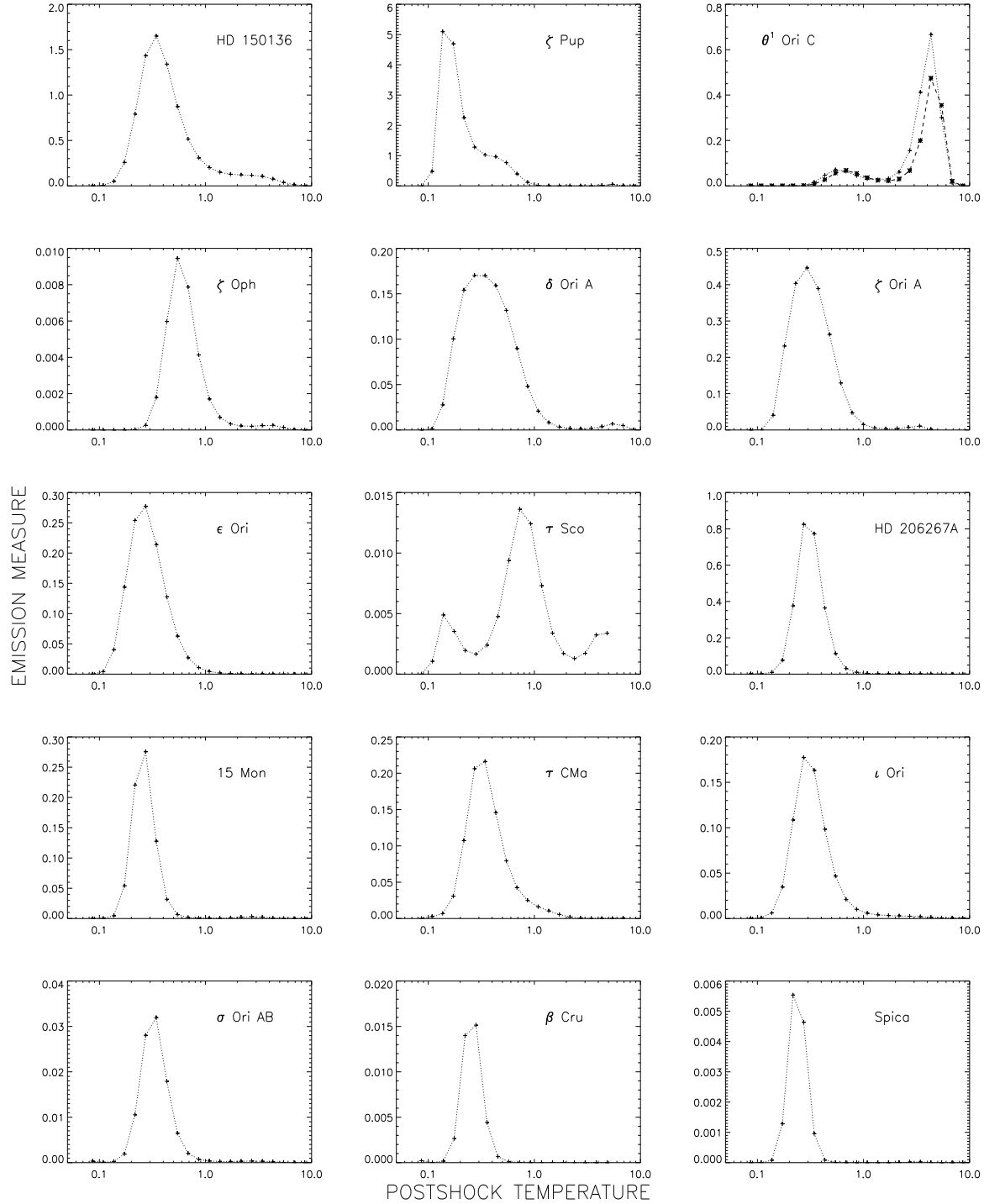


Figure 2. Emission measure distribution of radiative shocks in the OB stars of our sample. **Horizontal axes** are the immediate postshock temperature in keV; **vertical axes** are the emission measure in units of 10^{56} cm^{-3} . In the case of θ^1 Ori C, the results for ObsId 3 and ObsId 4 are shown by dotted and dashed lines, respectively.

quantity δ) and the cold-gas density. The latter is proportional to the density of the smooth stellar wind, that is to the ratio of the mass loss to the wind velocity. Thus, one can use the total stellar ‘cloudiness’² in a given object, given

sure of radiative shocks is derived from the spectral fit of a given star. This yields the values of Γ_{sh} for each temperature (T_{sh}). Then, based on eq. (A1) these values are used to derive the corresponding specific ‘cloudiness’ (δ) for each radiative shock in the distribution. Finally, the individual δ -values are added to give the total stellar ‘cloudiness’ for the studied object.

² Total stellar ‘cloudiness’: The distribution of emission mea-

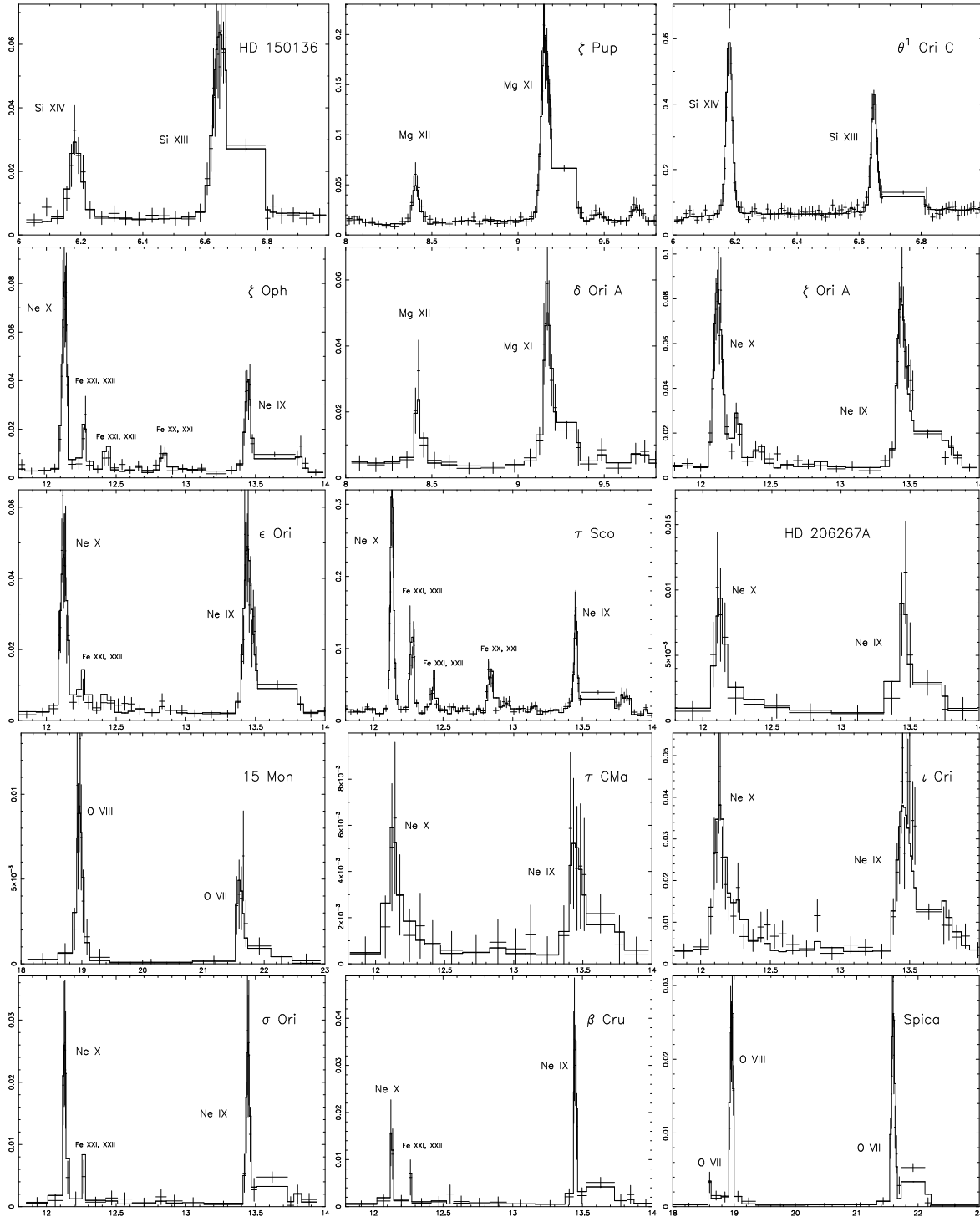


Figure 3. Portion of the background-subtracted spectra near some strong emission lines. The overlaid best-fit model is also shown (solid line). **Horizontal axes** are the observed wavelength (\AA); **vertical axes** are the flux density ($\text{photons s}^{-1} \text{\AA}^{-1}$).

by the sum of all the specific values, as a measure of the overall efficiency of the cold X-ray absorbers in the wind. In such a case, a correlation between the total ‘cloudiness’ and the line shift of the spectral lines should be expected, in the sense that the larger the total ‘cloudiness’, the higher the amount of blue-shift of the X-ray spectrum of the star.

Figure 4 presents the results of our estimate of the total stellar ‘cloudiness’ vs. the global line shifts in the X-ray

spectra of the massive stars of our sample. These results indicate that the expected correlation does exist: winds from stars with high values of the covering factor display a larger amount of blue-shift in the X-ray line profiles. Note that for many objects the derived from the fit errors can be appreciable. Unfortunately, the complexity of the model fits and the non-uniform quality of the data limit the accuracy on the derivation of the plotted quantities. An additional

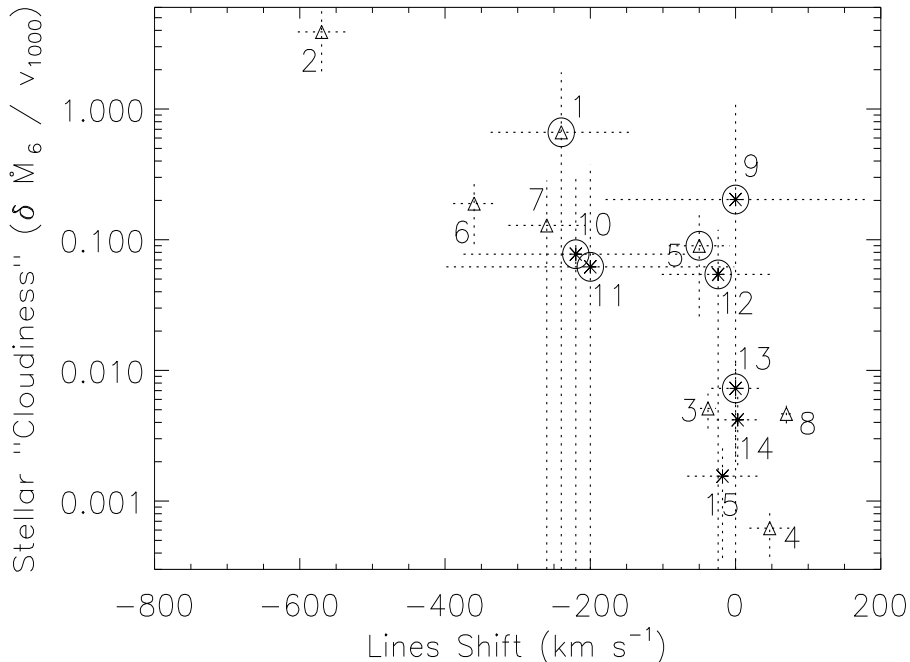


Figure 4. Total stellar ‘cloudiness’ vs. global line shift for the OB stars of the sample. The error bars (dotted lines) are 1σ errors from the fit (the errors of the total stellar ‘cloudiness’ follow from the 1σ errors for the total emission measure as derived in the fit, and the uncertainties of the distance to the studied object are not taken into account in the error propagation). The objects with good photon statistics (total number of counts in the spectrum higher than 5000) are marked by triangles. Data points within circles are binaries or multiple systems (as identified in SIMBAD). Stars are identified by numbers as in Table 1. The data point for θ^1 Ori C (number 3) is the average of the two observations.

source of uncertainty comes from the ‘cloudiness’ parameter that depends on the accuracy of the cooling curve (see eq. 5). However, the key point is that all the objects were analyzed in a uniform way. Thus, future improvements in the atomic data (i.e. cooling curve) might only shift the scale, but they will not affect the observed trend that we believe is rather robust. More importantly, as can be seen in Fig. 4 appreciable red shifts of the spectral lines are not observed.

The observed correlation between the total stellar ‘cloudiness’ and the spectral line shifts reveals additional details about the X-ray emitting zone in hot massive stars. For example, from Fig. 4 and for typical mass-loss rates ($\dot{M}_6 \approx 0.1 - 1$) and wind velocities ($v_{1000} \approx 1.5 - 2.5$), in most cases the ‘cloudiness’ parameter is small ($\delta \leq 1$). In other words, dense clumps/clouds do not completely cover the X-ray ‘sky’ of massive stars. This also means that the RDI instabilities (and the MCWS as well) do not affect a big part of their stellar winds.

Comparing the results for single and multiple systems, we note that the latter show higher values of the ‘cloudiness’ parameter: this could result from additional sources of X-ray emission, such as colliding wind shocks in binary stars (Luo, McCray & MacLow 1990; Stevens, Blondin & Pollock 1992; Myasnikov & Zhekov 1993). We have to keep in mind that the ‘cloudiness’ parameter is also a measure of the efficiency of the X-ray production. Therefore, if an extra source of X-rays exists in some object, then it will result in an effectively larger

number of shocks representing the additional emission. This is the case for a binary system, where a higher value of that parameter is expected in comparison to a single star with the same spectral line shift.

Finally, the fact that no appreciable redshift of the X-ray line profiles is observed in any object indicates that the distribution of the absorbers in OB stars likely has a spherical (or axial) symmetry. Future observations with a high spectral resolution and a good photon statistics will give us an opportunity to further test these conclusions and to study the X-ray gas kinematics in greater detail. They will also show whether the ‘cloudiness’ parameter for a given object changes with time which might be an important characteristic of the mechanism that drives the wind instabilities responsible for the X-ray emission from massive stars.

6 CONCLUSIONS

Using the *Chandra* public archive, we have analyzed the X-ray spectra of a sample of 15 massive OB stars. The basic assumption in this study is that the X-ray emission from such objects originates in shocks which develop in the stellar wind either as a result of radiation-driven instabilities or due to confinement of the wind by relatively strong magnetic field. The main results and conclusions are as follows:

1. Based on the fast shock cooling in the winds of hot massive stars, we have developed a simple model of a steady-

state, plane-parallel radiative shock which has been incorporated in the software package for analysis of X-ray spectra, XSPEC .

2. The model is then used in a global analysis of the X-ray emission from the sample of OB stars with high quality spectra obtained by *Chandra*. We assume that the X-ray emission originates from an ensemble of shocks that are most efficient in the acceleration zone of the stellar wind. Far from the formation region the shock structures (clumps, complete or fractional shells) cool down and eventually become ‘cold’ clouds in the X-ray sky of the star. In case of high coverage, these clouds can effectively absorb the X-rays emitted by the underlying shocks. In such a case, the spectral lines in the X-ray spectrum of the massive star will be blue-shifted.

3. Using our model, we define a new quantity, the stellar ‘cloudiness’, which represents the X-ray absorption efficiency by the clouds in the stellar wind. Our analysis reveals that despite the large intrinsic uncertainties, there is a correlation between the stellar ‘cloudiness’ and the global line blue-shifts in the observed X-ray spectra of the sample stars.

4. For each star the model gives the distribution of emission measure (DEM) of the radiative shocks responsible for the observed X-rays. The sample of OB stars with good spectra is distinguished in two groups: (i) one with the DEM peaked at $\sim 0.1-0.4$ keV and with a very low level of high energy tail above 1.0 keV; (ii) one with the maximum of the DEM that falls at considerably higher temperatures. In the former case, the radiative-driven instability shocks are the likely mechanism for the production of X-rays, while in the latter (θ^1 Ori C, τ Sco and ζ Oph) the X-ray emission originates in magnetically-confined wind shocks.

5. The derivation of metal abundance indicates a sub-solar metallicity for all the stars of the sample, with iron a factor of 2-3 below the solar value.

7 ACKNOWLEDGMENTS

Partial financial support from the Bulgarian Academy of Sciences - Consiglio Nazionale delle Ricerche bilateral co-operation programme is acknowledged. This research has made use of the NASA’s Astrophysics Data System, and the SIMBAD astronomical database operated by CDS at Strasbourg, France.

REFERENCES

- Arnaud, K. A. 1996, in *Astronomical Data Analysis Software and Systems*, ed. G. Jacoby & J. Barnes (San Francisco:ASP), 17
- Anders, E. & Grevesse, N. 1989, *Geochimica et Cosmochimica Acta*, 53, 197
- Babel, J., & Montmerle, T. 1997, *ApJ*, 485, L29
- Berghöfer, T. W., Schmitt, J. H. M. M., & Cassinelli, J. P. 1996, *A&ASS*, 118, 481
- Cassinelli, J. P., Miller, N. A., Waldron, W. L., MacFarlane, J. J., & Cohen, D. H. 2001, *ApJ*, 554, L55
- Castor, J. I., Abbott, D. C. & Klein, R. I. 1975, *ApJ*, 195, 157
- Cohen, D. H., de Messieres, G. E., MacFarlane, J. J., Miller, N. A., Cassinelli, J. P., Owocki, S. P., & Liedahl, D. A. 2003, *ApJ*, 586, 495
- Cohen, D. H., Leutenegger, M. A., Grizzard, K. T., Reed, C. L., Kramer, R. H., & Owocki, S. P. 2006, *MNRAS*, 368, 1905
- Feldmeier, A., Oskinova, L., & Hamann, W.-R. 2003, *A&A*, 403, 217
- Feldmeier, A., Puls, J., & Pauldrach, A. W. A. 1997, *A&A*, 322, 878
- Gagne, M., Oksala, M. E., Cohen, D. H., Tonnesen, S. K.; ud-Doula, A., Owocki, S. P., Townsend, R. H. D., & MacFarlane, J. J. 2005, *ApJ*, 628, 986
- Gorenstein, P. 1975, *ApJ*, 98, 95
- Herbst, W., & Havlen, R. J. 1977, *A&ASS*, 30, 279
- Hoogerwerf, R., de Bruijne, J. H. J., & de Zeeuw, P. T. 2001, *A&A*, 365, 49
- Ignace, R. 2001, *ApJ*, 549, L119
- Kahn, S. M., Leutenegger, M. A., Cottam, J., Rauw, G., Vreux, J.-M., den Boggende, A. J. F., Mewe, R., & Güdel, M. 2001, *A&A*, 365, L312
- Kramer, R. H., Cohen, D. H., & Owocki, S. P. 2003, *ApJ*, 592, 532
- Kudritzki, R. P., Palsa, R., Feldmeier, A., Puls, J., & Pauldrach, A. W. A. 1996, *MPE Report* 263, 9
- Lemen, J. R., Mewe, R., Schrijver, C. J., & Fludra, A. 1989, *ApJ*, 341, 474
- Leutenegger, M. A., Paerels, F. B. S., Kahn, S. M., & Cohen, D. H. 2006, *ApJ*, 650, 1096
- Lucy, L.B. 1982, *ApJ*, 255, 286
- Lucy, L.B., & White, R.L. 1980, *ApJ*, 241, 300
- Luo, D., McCray, R. & MacLow, M.-M. 1990, *ApJ*, 362, 267
- Miller, N. A., Cassinelli, J. P., Waldron, W. L., MacFarlane, J. J., & Cohen, D. H. 2002, *ApJ*, 577, 951
- Morrison, R. & McCammon, D. 1983, *ApJ*, 270, 119
- Myasnikov, A.V. & Zhekov, S.A. 1993, *MNRAS*, 260, 221
- Myasnikov, A. V., Zhekov, S. A., & Belov, N. A. 1998, *MNRAS*, 298, 1021
- Oskinova, L. M., Feldmeier, A., & Hamann, W.-R. 2004, *A&A*, 422, 675
- Oskinova, L. M., Feldmeier, A., & Hamann, W.-R. 2006, *MNRAS*, 372, 313
- Owocki, S. P., & Cohen, D. H. 2001, *ApJ*, 559, 1108
- Owocki, S. P., & Cohen, D. H. 2006, *ApJ*, 648, 565
- Owocki, S. P., & Rybicki, G. B. 1984, *ApJ*, 284, 337
- Owocki, S. P., Castor, J. I., & Rybicki, G. B. 1988, *ApJ*, 335, 914
- Paerels, F. B. S., & Kahn, S. M. 2003, *ARAA*, 41, 291
- Raymond, J. C., Cox, D. P., & Smith, B. W. 1976, *ApJ*, 204, 290
- Sanz-Forcada, J., Franciosini, E., & Pallavicini, R. 2004, *A&A*, 421, 715
- Schulz, N. S. 2003, *Rev. Mex. AA*, 15, 220
- Schulz, N. S., Canizares, C. R., Huenemoerder, D., & Lee, J. C. 2000, *ApJ*, 545, L135
- Schulz, N. S., Canizares, C., Huenemoerder, D., & Tibbets, K. 2003, *ApJ*, 595, 365
- Skinner, S. L., Zhekov, S. A., Palla, F., & Barbosa, C. L. D. R. 2005, *MNRAS*, 361, 191
- Stevens, I. R., Blondin, J.M. & Pollock, A. M. T. 1992, *ApJ*, 386, 265
- ud-Doula, A., & Owocki, S. P. 2002, *ApJ*, 576, 413

- Waldron, W. L. & Cassinelli, J. P. 2000, ApJ, 548, L45
Wojdowski, P. S. & Schulz, N. S. 2004, ApJ, 616, 630
Wojdowski, P. S. & Schulz, N. S. 2005, ApJ, 627, 953
Zhekov, S. A., McCray, R., Borkowski, K. J., Burrows, D. N., & Park, S. 2006, ApJ, 645, 293

APPENDIX A: THE MODEL

The physical background of the radiative shock model was given in § 2 along with the basic features of our global model that assumes a distribution of radiative shocks in the stellar wind of massive OB stars. Some technical details about these two models are described in this Appendix.

Shock Model: As discussed in § 2.1, the X-ray spectrum of a parcel of gas downstream from the shock front is given by the emission from an optically-thin plasma in CIE. Thus, the total spectrum of a radiative shock is an integral over a range of plasma temperatures, $T \leq T_{sh}$, in the cooling zone (see eq. [5]), where T_{sh} is the immediate postshock temperature for a strong shock. As seen from eq. (5), the emission measure in the cooling zone is a power-law function of temperature, T , and the spectrum at each value of T is assumed to be that given by the *vapex* model in XSPEC. The technical realization is based on the XSPEC subroutine *sumdem* with the APEC switch ON. For convenience, the numerical integration is over common logarithms ($d \lg T$). The X-ray emission from plasma cooler than $\sim 300,000$ K is not taken into account.

Thus, our XSPEC model of the X-ray emission from a radiative shock has the following parameters: the postshock temperature T_{sh} , chemical abundances, and the normalization factor Γ_{sh} . As for all optically-thin plasma models in XSPEC, the model normalization is related to the emission measure of the hot plasma and in this case Γ_{sh} gives the total EM in a radiative shock (for temperatures $T \leq T_{sh}$).

Global Model: Our global model assumes that the X-rays from massive OB stars originate in an ensemble of radiative shocks (§ 2.2). We use Chebyshev polynomials algorithm (Lemen et al. 1989) to describe the smoothed distribution of the emission measure in this ensemble of shocks. Since the basic parameter for shocks is the immediate postshock temperature, this distribution is computed relative to T_{sh} . Thus, the *total* EM in each shock of the ensemble is derived from the spectral fits. Note that the situation is similar in the XSPEC model *c6pvmkl* (which is based on Lemen et al. 1989) where the basic vectors are those giving the X-ray emission (spectrum) from optically-thin plasma in CIE. Here, the difference is that at each temperature T_{sh} we have the X-ray spectrum from a radiative shock, as described in § 2.1 and above. In the technical realization of the global shock model the total X-ray spectrum is derived by integrating the spectra from radiative shocks over the range of postshock temperatures. For convenience, this integration is over common logarithms ($d \lg T_{sh}$).

It should be noted that there is one important qualitative difference between the use of the global shock model or the model with distribution of emission measure of optically-thin plasma (e.g., *c6pvmkl* in XSPEC) for interpreting the observed X-ray spectra. In the former case, the EM at a given temperature, T_{sh} , in the distribution is the total EM (including plasma with $T \leq T_{sh}$) in a radiative shock with

velocity corresponding to this postshock temperature. In the latter case, the EM is that of an isothermal hot gas at that given temperature in the distribution. If an object is studied whose X-ray emission originates in radiative shocks, as is the case of massive OB stars, and a model like *c6pvmkl* in XSPEC is adopted, it is not quite correct to assign a shock velocity to each temperature value in the hot-gas distribution. This is because the hot plasma in a radiative shock is not isothermal (§ 2.1). Thus, the amount of hot gas at each temperature in the *c6pvmkl* distribution is the total contribution from all radiative shocks having some plasma at that temperature. This limitation is not present in our global shock model discussed in this work.

Additional advantage of the radiative shock model is that its normalization factor, Γ_{sh} , which gives the total emission measure in the shock, can be expressed through some of the basic shock parameters (as done in deriving eq. [5] using eq. [3]). In the simplified picture of spherically-symmetric stellar winds, it is justified to assume that the shocks move radially, and their surface can be presented as a fraction, δ , of the ‘local’ sphere: $A = \delta 4\pi R^2$. Thus, the normalization parameter, Γ_{sh} , of our XSPEC model can be written:

$$\begin{aligned} \Gamma_{sh} &= \frac{5A(1+x_e)n_{sh}v_{sh}k}{2\Lambda_0} \frac{10^{-14}}{4\pi d^2} \\ &= 2.444 \delta \left(\frac{\dot{M}_6}{v_{1000}} \right) \frac{\sqrt{T_{sh}}}{d_{kpc}^2} \end{aligned} \quad (A1)$$

where d_{kpc} is the distance to the object in kpc, and all other quantities are defined in § 2. The quantity $(10^{-14}/4\pi d^2)$ comes from the XSPEC normalization factor of the flux for optically-thin plasma models. Note that Γ_{sh} does not depend on the shock radius since in the case under consideration the gas density, n_{sh} , goes as R^{-2} . Again, the relative number density of hydrogen is assumed $x_H = 0.9$ and $x_e = 1.1$ for a fully ionized plasma. For simplicity, in deriving eq. (A1) we replaced the local wind velocity with the terminal speed which means that the effective surface of the shock (presented by δ) has the ‘maximum’ value. We note that the quantity δ may have values larger than unity since it represents the total area of the shocks with a particular velocity within the entire ensemble of shocks. Thus, once the value of the flux normalization parameter, Γ_{sh} , is derived from a spectral fit, it can be further used to gain insight into the physical picture, provided some of the stellar parameters are already known from other studies.